

ORIGINAL ARTICLE

Time–frequency analysis of differences between coordinates of three permanent GNSS stations in Krakow

Wiesław Kosek  ^{1*} and Zbigniew Siejka  ²¹Department of Environmental Engineering and Geodesy, Faculty of Production Engineering, University of Life Sciences in Lublin, 13 Akademicka Str, 20–950 Lublin, Poland²Department of Geodesy, Faculty of Environmental Engineering and Land Surveying, University of Agriculture in Krakow, Al. Mickiewicza 24/28, 30–059 Kraków, Poland

*wieslaw.kosek@up.lublin.pl

Abstract

This paper applies time–frequency analysis to a 3-day time series with a sampling interval of 1 second of the changes in E, N and H coordinates of three permanent GNSS stations: WRON, KR10, and KRUR in Krakow, as well as differences between them. Time–frequency analysis was conducted using a Fourier transform band–pass filter, which separates time series into frequency components. By analyzing the differences between these coordinates, it was observed that the WRON station shows a systematic error in the form of a regular wideband oscillation with a period of 75 minutes, whose amplitude varies from approximately 1 to 3 mm with a period of about 1 day. In the horizontal plane, this oscillation takes the shape of a flattened ellipse with a semi-major axis oriented in the northwest direction. The most probable cause of this regular oscillation is the day-to-day variability of the multipath signal environment.

Key words: GNSS, precise GBAS, multipath environment, Fourier transform filter

Highlights

- Three nearby GNSS stations in Kraków are similarly affected by local atmospheric effects or satellite constellation changes.
- Differences between station coordinates reveal systematic variations due to local effects, detectable by time–frequency analysis.
- Local effects could be affected by the variability of the multipath environment.

1 Introduction

Precise positioning using Global Navigation Satellite Systems (GNSS) supported by the multifunctional Ground–Based Augmentation System (GBAS) has become a fundamental tech-

nique for static and quick kinematic measurements in geodesy and various sectors of the economy in the 21st century. Currently, four global and two regional autonomous navigation systems, which are continuously expanding and modernizing, coexist (Cai and Gao, 2013). The four global GNSS that provide positioning and timing information worldwide are as follows:

- a) GPS (Global Positioning System), developed and operated by the United States government since the mid–1990s.
- b) GLONASS (rus. Globalnaja Navigacionnaja Sputnikowa Sistema), developed and operated by the Russian government. It initially achieved full operational capability in December 1995 and operated successfully until 2001. However, due to the shorter–than–expected lifespan of satellites and economic challenges in Russia, it lost full operational capability for over a decade, regaining it in December 2015.
- c) Galileo, developed by the European Union, was launched in

Table 1. List of GNSS satellites and their transmitted signals (as of October 17, 2023) – own study based on <https://qzss.go.jp>, <https://www.isro.gov.in>, <https://www.gsc-europa.eu>

GNSS	Constellation status		MEO	Orbit type*		Signals
	Total number of satellites	Number of operational satellites		GEO	IGSO/QZO	
GPS	31	29	31	–	–	L1C/A, L1C, L2C, L2E, L5
GLONASS	24	24	24	–	–	G1C, G2C, L3
Galileo	28	24	28	–	–	E1, E5a, E5b, E6
BeiDou	50	44	29	9	12	B1, B2, B3
QZSS	5	4	–	1	4	L1C/A, L1C, L2C, L5, L1S, L5S, L6
NAVIC/IRNSS	8	8	–	4	4	L5, S
Total	146	132	112	14	20	

* Orbit Type: MEO – Medium Earth Orbit, GEO – Geostationary Orbit, IGSO – Inclined Geosynchronous Orbit, QZO – Quasi Zenith Orbit.

December 2016, and is operated by the European Space Agency (ESA).

d) BeiDou, developed and operated by the Chinese government, has been fully operational since mid-2020.

The regional systems consist of the Japanese QZSS (Quasi Zenith Satellite System) and the NAVIC/IRNSS (NAVigation with Indian Constellation / Indian Regional Navigation Satellite System). The constellation of multi-GNSS navigation satellites consists of over 130 active satellites, distributed among four different types of orbits operating in multiple frequency bands, typically including L-band, S-band, and C-band (Table 1). The signals containing information about the satellite location, time, and other parameters, which the GNSS receiver uses to calculate its position on the Earth's surface, are transmitted at low power and are susceptible to interference and attenuation, which can affect the accuracy and reliability of the positioning information.

It is worth noting that GNSS satellites are equipped with different types of atomic clocks used to measure time, including RB (Rubidium), CS (Cesium), PHM (Passive Hydrogen Maser), RAFS (Rubidium Atomic Frequency Standard), and HMAC (Hydrogen Maser Atomic Clock), e.g., (Leick et al., 2015).

The use of a multi-GNSS solution, which involves combining signals from multiple GNSSs, can significantly improve satellite conditions at an observation site. This improvement is attributed to four main factors: 1) increased number of satellites, enhancing the reliability and accuracy of the positioning solution, 2) improved satellite geometry, providing a better spread of signals, 3) reduced impact of system failures and 4) enhanced availability of positioning information in areas with poor satellite visibility.

Working with multiple GNSSs simultaneously allows for very precise real-time positioning (at the centimeter level) with high time resolution (1 second or higher) due to shorter convergence time. Convergence time refers to the time required for the receiver to achieve a stable and accurate position fix after being turned on or after losing its fix due to obstructions or other issues. Various factors can affect convergence time, such as the quality and stability of the receiver internal clock, satellite signal strength and geometry, and the presence of signal reflections or obstructions.

Overall, adopting a multi-GNSS solution can significantly reduce convergence time by up to 70% and improves positioning accuracy by approximately 25%, eliminating some outliers (Li et al., 2015). Moreover, it is well-known that the availability and reliability of precise positioning using a single GNSS significantly decrease with increasing horizon cut angle. When the horizon truncation angle is set to 40°, the solution availabil-

ity rate drops to 40%. This reduction is particularly relevant to positioning and navigation in mountainous areas and urban canyons. On the other hand, a multi-GNSS solution can provide accurate positioning with an availability rate of over 95% (Li et al., 2015).

The weighting of multi-GNSS observations based on satellite orbit quality in real-time Precise Point Positioning (PPP) allows for a reduction of formal errors by 40%, for shortening convergence time by 40% and 47% for horizontal and vertical components, respectively, as well as for improving coordinate repeatability by 6% (Kazmierski et al., 2018). Parvazi et al. (2020) applied the recursive least squares method to determine the stochastic model of GNSS observations in solving the PPP problem and concluded that when multi-GNSS observations are combined, the lowest root mean square errors are estimated for the coordinate components.

Faster convergence times are achieved when a GNSS receiver receives signals with a high signal-to-noise ratio SNR (Richardson et al., 2016). The relationship between SNR and convergence time can be influenced by various factors, including the receiver sensitivity, antenna quality, atmospheric conditions, and obstructions. In the presence of obstructions or poor atmospheric conditions, lower SNR levels may result in longer convergence times. SNR is also impacted by multipath effects in GNSS code and phase measurements. Several studies have shown a strong correlation between SNR and multipath in these measurements (Axelrad et al., 1994, 1996; Strode and Groves, 2016; Špánik and Hefty, 2017; Peppas et al., 2019; Prochniewicz and Grzymala, 2021; Peppas and Psimoulis, 2023).

Lau and Cross (2005) described a multipath mitigation technique that uses SNR to estimate phase errors in measurements contaminated by multipath, and these estimates are applied for real-time correction before data processing. The approach proposed by Han et al. (2019), involving an SNR-dependent environment model in real-time GNSS landslide monitoring, when compared with the results of the classical model, could significantly improve precision at the millimeter level and reduce convergence time to a few seconds, ensuring continuous and reliable positioning results.

In general, the convergence time for GNSS receivers has been decreasing over the years with the introduction of newer and more advanced satellite constellations and receiver technologies (Siejka, 2018).

GBAS is a technology used to improve the accuracy, availability, and integrity of GNSS. It involves a network of ground-based reference stations that precisely measure errors in GNSS signals and broadcast this information to users within the coverage area. Using the correction data provided by GBAS, users can compensate for errors in the GNSS signals and improve the

accuracy of their positioning information. To achieve the highest possible accuracy for a user's coordinates, the coordinates of the GBAS stations must be stable and accurate.

2 Preliminary analysis

The GBAS stations selected for analysis are in close proximity to each other in Kraków and are named KRUR at 253c Balicka Street, KR10 at 36 Centralna Street, and WRON at 3 Wrońskiego Street. The KR10 station is owned by the commercial company VRSNet.pl Sp. z o.o. (Virtual Reference Station Net Limited Liability Company) in Kraków. The KRUR station is a scientific research station affiliated with the University of Agriculture in Kraków, while the WRON station operates as a private reference station. The measurements were taken during a period when maintenance work was being carried out on the KRUR and KR10 stations, which involved replacing GNSS antennas. Identical multi-system 440-channel receivers, Trimble R10 model 2, integrated with GNSS antennas, were installed at all these stations for the purpose of this experiment. These receivers are capable of tracking all available navigation systems and signals listed in Table 1. This proximity ensures that the stations will use the same GNSS satellites to determine their coordinates and that any systematic errors caused by the tropospheric and ionospheric conditions will be the same. In this study, short-term oscillations in the N (north), E (east), and H (height) components were investigated. The analysis were based on high-frequency kinematic GNSS observations conducted in real-time, with a 1-second sampling interval, during the period from April 3rd to April 5th, 2021. This experiment was conducted exclusively for this study at reference stations. Typically, these stations operate as reference stations in static mode, generating time series with 1-hour sampling intervals to support various GBAS systems. Over the course of 3 days, nearly $n = 259,200$ time series points were observed at each station. The distances and azimuths between the KRUR-KR10, KR10-WRON, and WRON-KRUR points are 11,516 m, 5,310 m, and 13,960 m, respectively, with corresponding azimuths of 99.18°, 173.00°, and 300.61°. Since the permanent stations considered are in close proximity, the paths of GPS, GLONASS, Galileo, and Beidou satellites, as illustrated in Figure 1, will be identical for all stations. During 3 days of observations, the average number of GNSS satellites observed to obtain a solution was 29 and varied from 12 to 36. After the period of the experiment, the reference stations returned to the static operational mode.

Unfortunately, there were two or three gaps in these observations, which for KRUR, KR10 and WRON stations were 35, 46, and 94 missing points, which is equal to 0.014%, 0.018%, and 0.036% of total number of data, respectively. To make these time series equidistant, the missing data were filled with zeros. To check if these time series as well as the differences between them are normally distributed the skewness and kurtosis were computed (Table 2). The normal distribution has a skewness of zero and kurtosis of three and there are no official rules about cut-off criteria of deviations of these values to indicate non-normality. A skewness value that is less than 2.0 and a kurtosis not exceeding 7.0 are considered normal (Kim, 2013). West et al. (1995) proposed a reference of substantial departure from normality as an absolute kurtosis value > 7.1 . According to these criteria, the analyzed time series as well as the differences between them meet the conditions for a normal distribution.

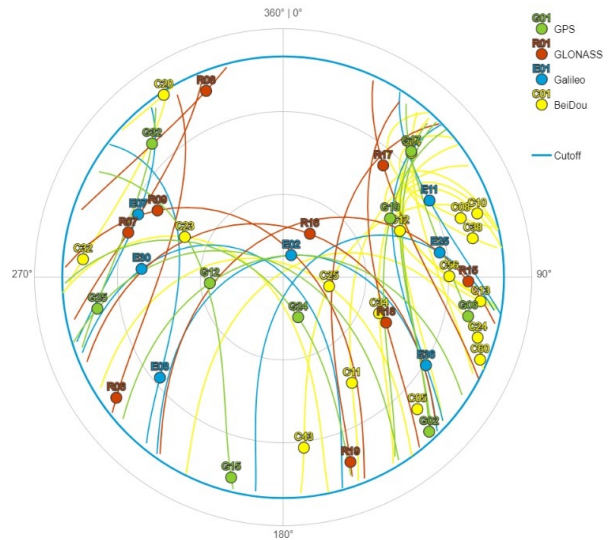


Figure 1. Sky plots azimuth vs. elevation for four GNSS, (GPS – in green, GLONASS – in red, Galileo – in blue, BeiDou – in yellow) – Station WRON date April 3, 2021

3 The Fourier transform band pass filter amplitude spectra

A wide-band oscillation computed by the Fourier transform band-pass filter (FTBPF) is given by the following formula (Kosek, 1995; Popiński and Kosek, 1995; Popiński, 2009):

$$x(t, \omega) = \text{FFT}^{-1} \{ \text{FFT} [x(t)] \cdot P(\mu, \omega) \} \quad (1)$$

where: FFT, FFT^{-1} are the fast Fourier transform and the inverse fast Fourier transform (Singleton, 1969) operators, respectively,

$$P(\mu, \omega) = \begin{cases} 1 - [(\omega - \mu)/\lambda]^2 & \text{for } |\omega - \mu| \leq \lambda \\ 0 & \text{for } |\omega - \mu| < \lambda \end{cases}$$

is the parabolic transmittance function in which μ is the frequency argument, $\omega = 2\pi/T$ is the central oscillation frequency, T is the central oscillation period, λ is half of the window bandwidth and $x(t) = x_1(t) + ix_2(t)$ is complex-valued or real-valued (if imaginary part $x_2(t) = 0$) time series, $i = \sqrt{-1}$. In this paper, the parameter $\lambda = 0.0005$ was adopted.

The wide band oscillation $x(k, \omega)$ can be then used to compute the time-frequency FTBPF spectrum by the following formula:

$$\hat{S}_{xx}(t, \omega) = \frac{1}{m} \sum_{k=-m/2}^{m/2} |x(k, \omega)|^2, \quad t = m/2+1, m/2+2, \dots, n-m/2 \quad (2)$$

where n is the total number of data, $m = jT/\Delta t$, $j = 2$, Δt is the sampling interval of data. The time-frequency FTBPF amplitude spectrum is defined as $\sqrt{2\hat{S}_{xx}(t, T)}$. The FTBPF amplitude spectrum $\sqrt{2\hat{S}_{xx}(T)}$ can be obtained when $m = n/2$.

4 Time-frequency analysis of GNSS station coordinates and differences between them

The FTBPF amplitude spectra of the N, E, and H components of GNSS observations at the KRUR, KR10, and WRON stations

Table 2. Standard deviation, skewness and kurtosis of KRUR, KR10 and WRON time series and the differences between them

GNSS Stations	Standard deviation [mm]			Skewness			Kurtosis		
	N	E	H	N	E	H	N	E	H
KRUR	3.7	2.9	8.6	0.050	0.051	-0.004	3.716	4.542	2.965
KR10	3.8	3.0	8.4	-0.068	0.251	0.107	3.318	4.308	3.129
WRON	4.3	3.9	10.0	-0.039	-0.142	0.081	2.837	3.209	2.967
KRUR-KR10	2.1	1.8	4.4	-0.062	-0.121	-0.239	3.603	3.796	3.594
WRON-KR10	2.7	2.8	5.9	-0.162	-0.091	0.168	2.748	2.871	3.264
WRON-KRUR	3.0	3.0	6.4	-0.016	0.056	0.130	3.169	2.882	3.094

The standard errors of skewness and kurtosis are equal to ± 0.0048 and ± 0.0096 , respectively.

indicate that the average amplitude of oscillations for periods shorter than 15 minutes in the N and E components is less than 0.5 mm, while for the H component it is less than 1 mm (Figure 2). Therefore, oscillations with periods shorter than 15 minutes in these components can be regarded as insignificant. To reduce the amount of data by ten times, interpolation of these time series was made every 10 seconds, with each interpolated point being the average of the 10-second time interval.

The amplitude spectra of the WRON time series in the N and E components show a peak for oscillations with a period of about 70 days with an average amplitude of the order of 2 mm. The amplitude spectra of the N and E components of the KRUR and KR10 time series do not show this peak and are very similar. In the case of the H component, the FTBPF amplitude spectra are of the same order and are very similar for the KRUR and KR10 stations (Figure 2).

To identify systematic errors in the individual KRUR, WRON, and KR10 stations, the differences between them were analyzed. The standard deviations of the differences were slightly smaller compared to those of the time series themselves (Table 2). The skewness and kurtosis values of the differences remained at the same level as those of the time series themselves.

The time-frequency FTBPF amplitude spectra of the differences between the WRON-KR10, WRON-KRUR, and KR10-KRUR time series for the N, E, and H components are shown in Figure 3. The time-frequency amplitude spectra of WRON-KR10 and WRON-KRUR differences had similar amplitude maxima separated by approximately one day for a given frequency band ranging from 50 to 150-minute oscillations. The maximum amplitude of the 75-minute oscillation was about 4 mm. The time-frequency FTBPF amplitude spectra of the KR10-KRUR differences in each component were much smaller than for the WRON-KR10 and WRON-KRUR differences, and the amplitude maxima did not exceed 1 mm for the N and E components and about 2 mm for the H component.

The FTBPF amplitude spectra of the differences between the WRON and KR10, WRON and KRUR time series in individual N, E, and H components (Figure 4) showed peaks for oscillations with a period of about 75 minutes and an average amplitude of 1.5, 1.8, and 2.5–3.0 mm, respectively. There were no significant peaks in the amplitude spectra of KRUR-KR10 differences in each component, and the mean amplitudes of all oscillations were around 0.5 mm for N and E components and 1.0 mm for the H component, which were about two times smaller than the mean amplitudes of all oscillations in the amplitude spectra of individual stations shown in Figure 2.

The FTBPF amplitude spectrum of the complex-valued $E+iN$ horizontal components for WRON-KR10 and WRON-KRUR differences indicates that the amplitude of the 75-minute oscillation is almost the same for both prograde and retrograde oscillations, at about 1.2 mm (Figure 5). This suggests that the 75-minute oscillation has a flattened ellipse shape.

Figure 6 shows the wideband 75-minute oscillations com-

puted by the FTBPF in each component of the WRON-KR10 and WRON-KRUR differences. The maxima of amplitudes in all components occur between 17:00 and 18:00 each day.

In the frequency band of the 75-minute oscillation in the horizontal plane of N and E coordinates for the WRON-KR10 and WRON-KRUR differences (Figure 7), the N and E components are opposite in phase, indicating that these vibrations occur in the northwest (or southeast) direction. The presence of this oscillation in these differences suggests that it results from systematic observation errors at the WRON station, possibly caused by changes in the instrumental-related issues of the GNSS antenna or other systematic factors related to this station.

Since the amplitude of the 75-day oscillation in the vertical axis H direction is almost twice as large as in the horizontal axes N and E directions, the semi-major axes of the ellipses in the NH and EH planes would be dominated by the direction of the H axis.

5 Discussion

There are several possible causes for a systematic oscillation observed in the horizontal components of a GNSS permanent station with a period of 75 minutes and variable amplitude. These include tidal deformation of Earth's crust (Baker, 1984; Piras et al., 2009), seismic waves from distant earthquakes causing periodic variations in the position of the GNSS station (Kouba, 2003; Ren et al., 2021), large-scale atmospheric pressure variations associated with weather systems, which can cause periodic variations of the Earth's crust, e.g. (Dach et al., 2011), and instrumental-related issues such as thermal expansion or mechanical vibrations in the station antenna, metal structures (Mohamed et al., 2019; Fuhrmann et al., 2021) or microwave-absorbing materials (Hunegnaw and Teferle, 2022) situated in the direct vicinity of a GNSS receiver antenna or multipath effects due to GNSS signals reflected from objects around the antenna interfering with direct signals from these satellites (Peppas et al., 2019). Peppas and Psimoulis (2023) attempted to model the multipath effect of GNSS signals using signal-to-noise ratio (SNR) measurements of GNSS signals. The proposed method for modelling this motion is based on the hypothesis that changes in the multipath effect can be expressed through SNR.

Tidal deformation of the Earth's crust, atmospheric pressure variations, or distant earthquakes would likely cause similar periodic changes at all three considered GNSS stations due to their close proximity. However, considering the proximity of the stations, it is more plausible that changes in the coordinates of one of the stations are related to instrumental issues with the GNSS antenna. Therefore, despite the GNSS antenna at the WRON station remaining stable during the recording period, the most probable cause of the 75-minute oscillation is the periodic change in the environmental multipath effect.

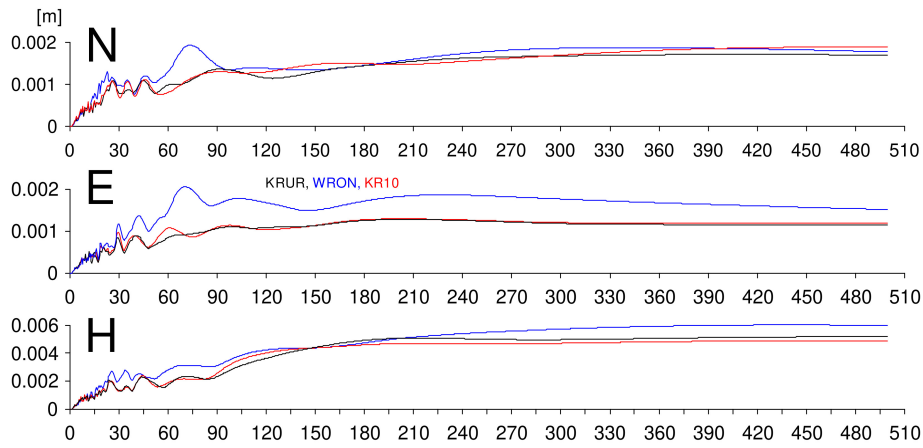


Figure 2. The FTBPF amplitude spectra of N, E and H components at WRON (blue line), KRUR (black line) and KR10 (red line) stations (period in minutes)

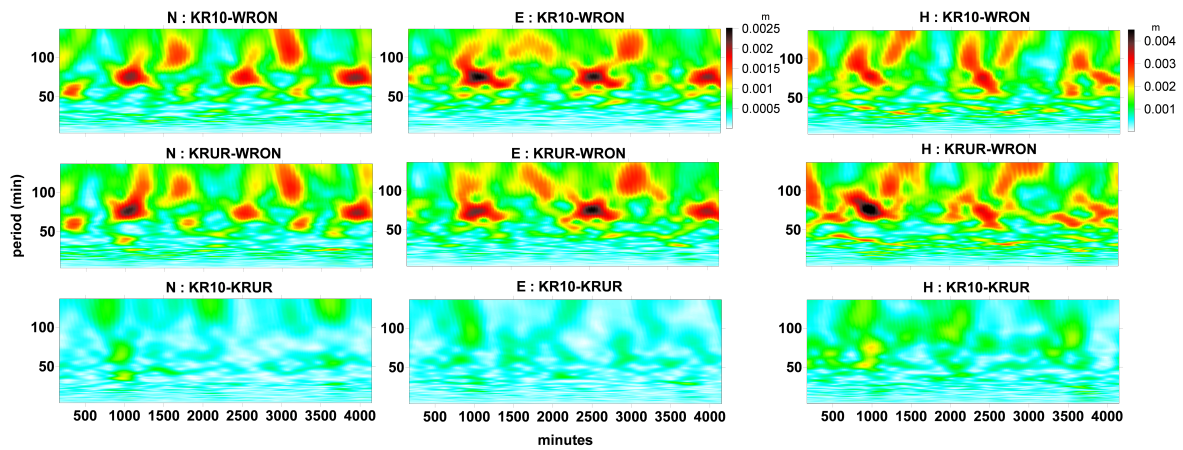


Figure 3. Time-frequency FTBPF amplitude spectra of WRON-KR10, WRON-KRUR, and KR10-KRUR differences in N, E and H components

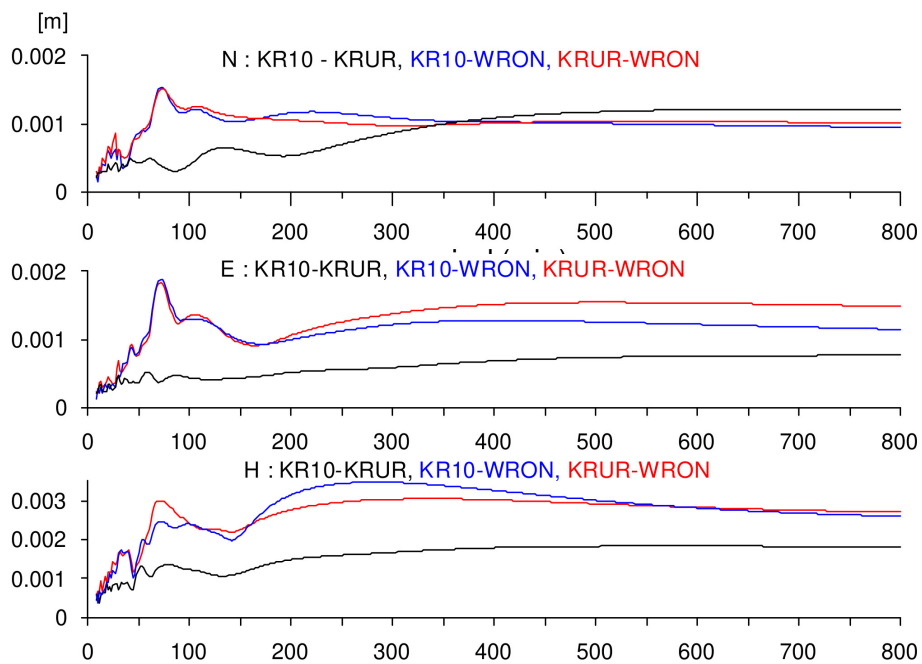


Figure 4. The FTBPF amplitude spectra of the WRON = KR10, WRON - KRUR, and KR10 - KRUR differences for N, E and H components (period in minutes)

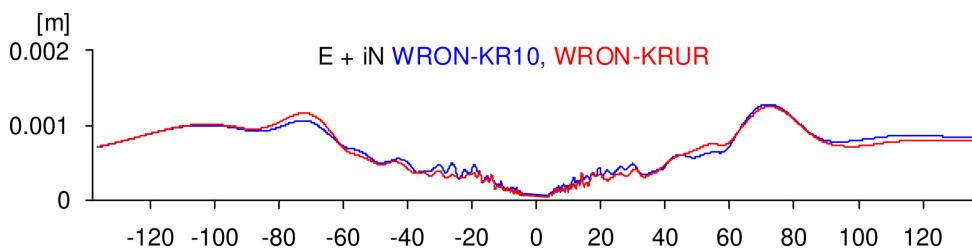


Figure 5. The FTBPF amplitude spectrum of complex-valued differences of E+iN components of WRON-KR10 and WRON-KRUR (period in minutes)

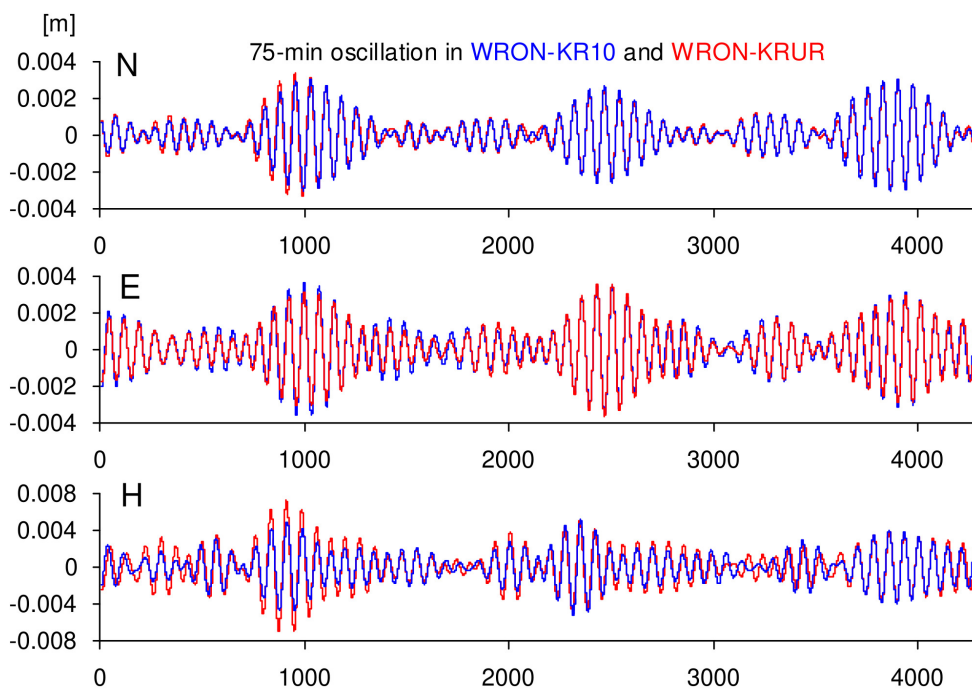


Figure 6. The 75-minute oscillation in the differences of WRON-KR10 (blue) and WRON-KRUR (red) for the N, E and H components (minutes since 3.04.2022)

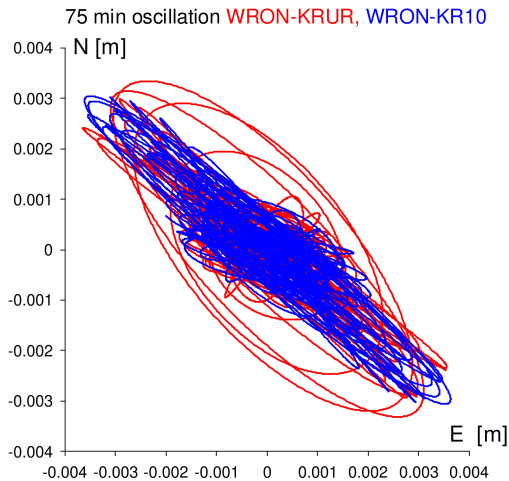


Figure 7. The 75-minute oscillation in the differences of WRON-KR10 (blue) and WRON-KRUR (red) in the horizontal NE plane.

6 Conclusions

Preliminary analysis using variance, skewness, and kurtosis computations of time series of coordinates of three permanent GNSS stations WRON, KRUR, and KR10 in Krakow and their differences showed that all these time series meet the conditions for a normal distribution. By analyzing these time series and corresponding differences between them using the FTBPF, it was observed that the WRON station shows a systematic error in the form of a wide-band regular 75-minute oscillation in the horizontal plane of N and E coordinates with a varying amplitude that varies with a period of 1 day. These 75-minute vibrations have the shape of a flattened ellipse with the semi-major axis pointed in the northwest direction.

The most probable cause of the regular 75-minute oscillation with daily amplitude variations at the WRON station is the day-to-day variability of the multipath environment, which can be modelled using SNR variations. Further analysis and investigation would be necessary to determine the most likely cause of the observed oscillation by investigating the multipath environment and the GNSS antenna oscillatory motion by modelling the SNR observables of GNSS signals.

Acknowledgments

The paper was sponsored by the statutory funds of the Faculty Production Engineering of the University of Life Sciences in Lublin and of the Faculty of Environmental Engineering and Land Surveying of the University of Agriculture in Krakow.

References

Axelrad, P., Comp, C., and MacDoran, P. (1994). Use of signal-to-noise ratio for multipath error correction in GPS differential phase measurements: methodology and experimental results. In *Proceedings of the 7th international technical meeting of the Satellite Division of The Institute of Navigation (ION GPS 1994)*, Salt Lake City, UT, September 1994, pages 655–666.

Axelrad, P., Comp, C. J., and Macdoran, P. F. (1996). SNR-based multipath error correction for GPS differential phase. *IEEE Transactions on Aerospace and Electronic Systems*, 32(2):650–660, doi:10.1109/7.489508.

Baker, T. (1984). Tidal deformations of the Earth. *Science Progress (1933-)*, pages 197–233.

Cai, C. and Gao, Y. (2013). Modeling and assessment of combined GPS/GLONASS precise point positioning. *GPS solutions*, 17:223–236, doi:10.1007/s10291-012-0273-9.

Dach, R., Böhm, J., Lutz, S., Steigenberger, P., and Beutler, G. (2011). Evaluation of the impact of atmospheric pressure loading modeling on GNSS data analysis. *Journal of geodesy*, 85:75–91, doi:10.1007/s00190-010-0417-z.

Fuhrmann, T., Garthwaite, M. C., and McClusky, S. (2021). Investigating GNSS multipath effects induced by co-located Radar Corner Reflectors. *Journal of Applied Geodesy*, 15(3):207–224, doi:10.1515/jag-2020-0040.

Han, J., Tu, R., Zhang, R., Fan, L., and Zhang, P. (2019). SNR-dependent environmental model: application in real-time GNSS landslide monitoring. *Sensors*, 19(22):5017, doi:10.3390/s19225017.

Hunegnaw, A. and Teferle, F. N. (2022). Evaluation of the multipath environment using electromagnetic-absorbing materials at continuous GNSS stations. *Sensors*, 22(9):3384, doi:10.3390/s22093384.

Kazmierski, K., Hadas, T., and Sońnica, K. (2018). Weighting of multi-GNSS observations in real-time precise point positioning. *Remote Sensing*, 10(1):84, doi:10.3390/rs10010084.

Kim, H.-Y. (2013). Statistical notes for clinical researchers: assessing normal distribution (2) using skewness and kurtosis. *Restorative dentistry & endodontics*, 38(1):52–54, doi:10.5395/rde.2013.38.1.52.

Kosek, W. (1995). Time variable band pass filter spectra of real and complex-valued polar motion series. *Artificial Satellites*, 30(1):27–43.

Kouba, J. (2003). Measuring seismic waves induced by large earthquakes with GPS. *Studia Geophysica et Geodaetica*, 47:741–755, doi:10.1023/A:1026390618355.

Lau, L. and Cross, P. (2005). Use of signal-to-noise ratios for real-time GNSS phase multipath mitigation. In *Proc. of National Navigation Conference NAV05, The Royal Institute of Navigation, 1–3 November 2005, London*, volume 1.

Leick, A., Rapoport, L., and Tatarnikov, D. (2015). *GPS satellite surveying*. John Wiley & Sons.

Li, X., Ge, M., Dai, X., Ren, X., Fritsche, M., Wickert, J., and Schuh, H. (2015). Accuracy and reliability of multi-GNSS real-time precise positioning: GPS, GLONASS, BeiDou, and Galileo. *Journal of geodesy*, 89(6):607–635, doi:10.1007/s00190-015-0802-8.

Mohamed, A. S., Doma, M. I., and Rabah, M. M. (2019). Study the effect of surrounding surface material types on the multipath of GPS signal and its impact on the accuracy of positioning determination. *American Journal of Geographic Information System*, 8(5):199–205, doi:10.5923/j.ajgis.20190805.01.

Parvazi, K., Farzaneh, S., and Safari, A. (2020). Role of the RLS-VCE-estimated stochastic model for improvement of accuracy and convergence time in multi-GNSS precise point positioning. *Measurement*, 165:108073, doi:10.1016/j.measurement.2020.108073.

Peppas, I. and Psimoulis, P. (2023). Detection of GNSS antenna oscillatory motion and multipath conditions via exploitation of multipath-induced SNR variations. *GPS Solutions*, 27(3):117, doi:10.1007/s10291-023-01432-6.

Peppas, I., Psimoulis, P., and Meng, X. (2019). Modelling antenna vibrations using the Signal-to-Noise Ratio (SNR) of GNSS signals. In *Proceeding of 4th joint international symposium on deformation monitoring (JISDM) Athe, 15–17 May 2019, Athens, Greece*.

Piras, M., Roggero, M., and Fantino, M. (2009). Crustal deformation monitoring by GNSS: network analysis and case studies. In *Advances in Geosciences: Volume 13: Solid Earth (SE)*, pages 87–103. World Scientific, doi:10.1142/9789812836182_0007.

- Popiński, W. (2009). On application of the Fourier transform band pass filtering technique. *Artificial Satellites*, 44(4):149–160, doi:10.2478/v10018-009-0026-3.
- Popiński, W. and Kosek, W. (1995). The Fourier transform band pass filter and its application for polar motion analysis. *Artificial Satellites*, 30(1):9–25.
- Prochniewicz, D. and Grzymala, M. (2021). Analysis of the impact of multipath on Galileo system measurements. *Remote Sensing*, 13(12):2295, doi:10.3390/rs13122295.
- Ren, Y., Lian, L., and Wang, J. (2021). Analysis of seismic deformation from global three-decade GNSS displacements: implications for a three-dimensional Earth GNSS velocity field. *Remote Sensing*, 13(17):3369, doi:10.3390/rs13173369.
- Richardson, T., Hill, C., Moore, T., and Toor, P. (2016). Analysis of multi-constellation GNSS signal quality. In *Proceedings of the 2016 International Technical Meeting of The Institute of Navigation, Monterey, California, January 2016*, pages 631–638. doi:10.33012/2016.13394.
- Siejka, Z. (2018). Validation of the accuracy and convergence time of Real Time Kinematic results using a single Galileo navigation system. *Sensors*, 18(8):2412, doi:10.3390/s18082412.
- Singleton, R. (1969). An algorithm for computing the mixed radix fast Fourier transform. *IEEE Transactions on audio and electroacoustics*, 17(2):93–103, doi:10.1109/TAU.1969.1162042.
- Špánik, P. and Hefty, J. (2017). Multipath detection with the combination of SNR measurements – example from urban environment. *Geodesy and Cartography*, 66(2), doi:10.1515/geocart-2017-0020.
- Strode, P. R. and Groves, P. D. (2016). GNSS multipath detection using three-frequency Signal-to-Noise measurements. *GPS solutions*, 20:399–412, doi:10.1007/s10291-015-0449-1.
- West, S. G., Finch, J. F., and Curran, P. J. (1995). Structural equation models with nonnormal variables: Problems and remedies. In Hoyle, R., editor, *Structural equation modeling: Concepts, issues and applications*, pages 56–75. Newbery Park, CA: Sage.